



Using thermodynamic integration MD simulation to compute relative protein–ligand binding free energy of a GSK3 β kinase inhibitor and its analogs

Hsing-Chou Lee, Wen-Chi Hsu, An-Lun Liu, Chia-Jen Hsu, Ying-Chieh Sun*

Department of Chemistry, National Taiwan Normal University, 88, TingChow Road Section 4, Taipei 116, Taiwan

ARTICLE INFO

Article history:

Accepted 22 April 2014

Available online 2 May 2014

Keywords:

Thermodynamic integration

MD simulation

Relative binding free energy

GSK3 β kinase

Inhibitor

ABSTRACT

Thermodynamic integration molecular dynamics simulation was used to investigate how TI-MD simulation preforms in reproducing relative protein–ligand binding free energy of a pair of analogous GSK3 β kinase inhibitors of available experimental data (see Fig. 1), and to predict the affinity for other analogs. The computation for the pair gave a $\Delta\Delta G$ of 1.0 kcal/mol, which was in reasonably good agreement with the experimental value of -0.1 kcal/mol. The error bar was estimated at 0.5 kcal/mol. Subsequently, we employed the same protocol to proceed with simulations to find analogous inhibitors with a stronger affinity. Four analogs with a substitution at one site inside the binding pocket were the first to be tried, but no significant enhancement in affinity was found. Subsequent simulations for another 7 analogs was focused on substitutions at the benzene ring of another site, which gave two analogs (analog 9 and 10) with $\Delta\Delta G$ values of -0.6 and -0.8 kcal/mol, respectively. Both analogs had a $-OH$ group at the meta position and another $-OH$ group at the ortho position at the other side of the benzene ring, as shown in Table 3. To explore further, another 4 analogs with this characteristic were investigated. Three analogs with $\Delta\Delta G$ values of -2.2 , -1.7 and -1.2 kcal/mol, respectively, were found. Hydrogen bond analysis suggested that the additional hydrogen bonds of the added $-OH$ groups with Gln185 and/or Asn64, which did not appear in the reference inhibitor or as an analog with one substitution only in the examined cases, were the main contributors to an enhanced affinity. A prediction for better inhibitors should interest experimentalists of enzyme and/or cell assays. Analysis of the interactions between GSK3 β kinase and the investigated analogs will be useful in the design of GSK3 β kinase inhibitors for compounds of this class.

© 2014 Elsevier Inc. All rights reserved.

1. Introduction

Many kinases play a significant role in cell signaling transduction and are important drug target proteins for a number of diseases including Alzheimer's disease, diabetes, and cancer. This is considered to be the second-most important drug target group among biomolecules of pharmaceutical interest [1]. The development of kinase inhibitors continues to attract attention in fundamental and pharmaceutical applications research.

Computer modeling has been widely used in both the design and discovery of small molecular enzyme inhibitors. With

competitive inhibition, estimating the binding affinity of small molecules is a key step in realizing both the design and the discovery of these molecules. Typically, one of two categories of techniques is used: docking computation and molecular dynamics (MD) simulation of alchemical free energy calculation [2], which are empirical and first-principle in nature, respectively. The former is fast and is used to screen a large amount of compounds. The latter is more accurate but requires a considerable amount of computer time. As computer power and methodology development have progressed, so has the role of MD simulation in drug design. Recent simulations have demonstrated that with MD simulation, accuracy has reached 1.4–2.5 and <3.0 kcal/mol based on the examined systems described in two recent review papers [2,3]. The advantages and disadvantages of several widely used computational methods have been summarized in recent review papers [2–10]. In addition, a number of simulations have been carried out to investigate various effects in the binding free energy of ligand–protein complexes

Abbreviations: Htp, 7-(4-hydroxyphenyl)-2-pyridin-4-yl-5h-thieno[3,2-c]pyridin-4-one; TI, thermodynamic integration; MD, molecular dynamics.

* Corresponding author. Tel.: +886 2 7734 6215.

E-mail address: sun@ntnu.edu.tw (Y.-C. Sun).

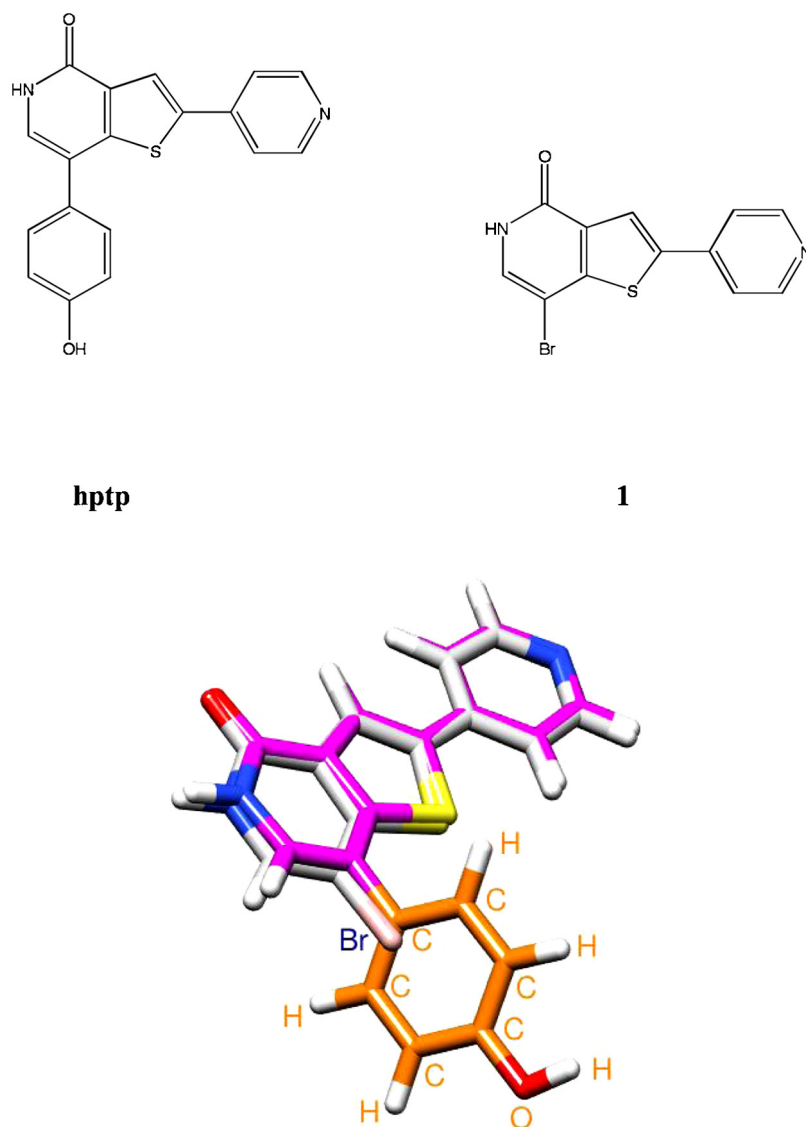


Fig. 1. Structure of the **hptp** compound and analog **1**. 3-Dimensional structures are shown in color (in magenta and light gray, respectively). The units of **hptp** that differ from those of **1** are highlighted in orange; these atoms are also labeled. Other color codes are the standard ones of Chimera [75], the graphic software used to produce this figure. Here, **hptp** is the reference ligand ($\lambda = 0$); **1** is the mutant ligand ($\lambda = 1$).

[11–55] (see also, for example, review articles [2–10] and references therein). Notably, a number of simulations have reached an accuracy of 0.5 kcal/mol (see, for example, these studies [36,44]). For kinases, an accuracy of ~ 0.5 kcal/mol for kinase–ligand complexes in excellent agreement with the experimental values was obtained in an earlier simulation with partial solvation at the binding site combined with structural restraints [11]. The continued development of sampling methods has improved sampling for protein–ligand complexes in the investigated cases [7,43–45]. In addition to these developments, a newly proposed framework of relative binding free energy calculation has laid out a promising scheme to enhance the convergence in computation [56]. With respect to the force field, sensitivity of the partial charges of an atom and van der Waals force field parameters on the computed binding free energy were computed and analyzed, which provided guidelines for improving force field parameters in alchemical free energy calculation [57]. Finally, in addition to these advances, a recently launched program, SAMPL [58,59], provides an excellent platform and blind test samples for the advancement of accuracy in the prediction of binding free energy. Along with the continued growth of computer power and improvement of computer codes

(see, for example, a recent article [55]), alchemical free energy calculation is expected to play a more important role in drug design and discovery.

In alchemical free energy calculation, absolute free energy calculation gives the absolute binding free energy of a protein–ligand complex for a single compound under investigation, which can be contrasted with relative binding free energy where only the relative binding free energy is determined for a pair of analogous compounds. In terms of the amount of computational power needed, in general, the latter is more affordable. The approach has been used to investigate protein/DNA–ligand binding for analogous compounds in a number of simulations [28–39,41,46–51]. The recent development of automation in free energy calculations has enhanced the versatility of relative binding free energy calculation [60].

Among existing kinase–inhibitor complexes of available experimental structure and affinity data, recent work on GSK3 β –inhibitor complexes provided an ideal case in investigating how TI MD simulation would perform on kinase–ligand complexes, because they have the same binding modes (see Fig. 1) [61]. Fig. 1 shows the structures of the two inhibitors. The **hptp** compound differs from its analog by the presence of a phenyl group where analog **1** is

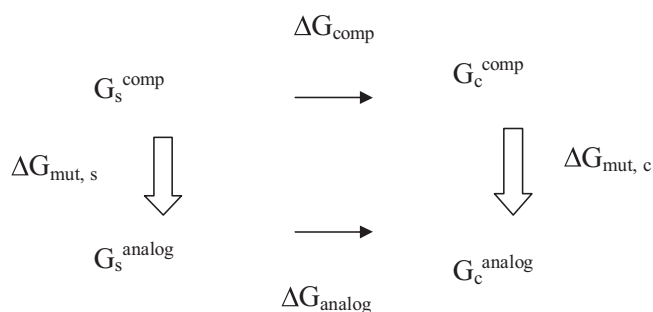


Fig. 2. Thermodynamic cycle of binding. comp denotes the reference compound (see text for detailed description).

substituted with a –Br group. The binding affinity measurement gave pIC50 values of 6.9 and 6.8 for compounds **hptp** and analog **1**, respectively, showing a similar binding affinity. In addition to its suitability to TI MD simulation, the GSK3 β kinase is also an important drug target protein for diabetes, Alzheimer's disease, and cancer [62]. Experimentally, a considerable amount of investigation has been conducted due to high pharmaceutical interest (see, for example, a review article [62] and the references therein). As for the theoretical aspect, number of theoretical investigations using simulation methods is relatively small. A few computational studies have provided theoretical insight into the effects of kinase activity [63–66]. In the present study, we applied TI MD simulation to see how it perform in reproducing experimental value. Our computation for the pair of available experimental data gave a relative binding free energy, $\Delta\Delta G$, of 1.0 kcal/mol, which was in reasonable agreement with the experimental value of –0.1 kcal/mol. The same computational protocol was therefore employed to predict the affinity of other analogs, with the aim of finding new analogous compounds with better affinity, and to understand the interactions between ligands of this class and GSK3 β kinase. Among the predicted 16 analogs, the simulations gave 5 analogs with a better affinity, which was ≥ 0.8 kcal/mol. Hydrogen bonding was examined in order to analyze the stabilizing factors in the enhanced affinity. These results should interest experimentalists for future study. The Formulation of the TI simulation is briefly introduced in the second section along with the simulation details. The results and discussion are both provided in Section 3. The final section contains concluding remarks.

2. Methods and computation

2.1. Formulation

The fundamental formulation and computational procedure for the free energy calculation can be found in a review paper [67]. The relative binding free energy ($\Delta\Delta G$) of a compound and its analog binding with a protein can be calculated using the thermodynamic cycle displayed in Fig. 2. The relative binding free energy, $\Delta G_{analog} - \Delta G_{comp}$, is equal to

$\Delta G_{mut,c} - \Delta G_{mut,s}$ where the subscripts “comp” and “analog” denote the reference compound and its analog, respectively. In this equation, “mut” is the mutational change and “c” and “s” represent the complex and solution states, respectively. The mutational free energy change is calculated using the following equation:

$$\Delta G_{mut} = \int_0^1 d\lambda \left\langle \frac{dV}{d\lambda} \right\rangle_\lambda$$

where λ is the mutational variable switching from 0 (reference state) to 1 (mutated state); $\langle \rangle_\lambda$ is the ensemble average of the calculated quantities sampled at the hybrid Hamiltonian at the specific value of λ , and $\langle dV/d\lambda \rangle_\lambda$ is calculated using MD simulation. In

practice, selected λ points are computed in MD simulations to give integrands at those λ points and are used in subsequent numerical integration to obtain ΔG_{mut} . In the present computation, the values were computed at values for λ of 0.1, 0.2, ..., 0.9. The values for λ of 0.0 and 1.0 were obtained through extrapolation, following the procedure described in the Amber11 manual [68].

2.2. Computation

The computational procedure was essentially the same as with our previous work [49]. Briefly, to compute $\Delta G_{mut,c}$ and $\Delta G_{mut,s}$, the modeling systems were prepared using the Amber11 package [68]; ΔG_{mut} is the mutational free energy change. For the complex state, the GSK3 β –**hptp** structure obtained from the protein databank (pdb code: 3zrm) was used as the initial structure. The resolution of the crystal structure was 2.49 Å. Two crystal water molecules in the binding pocket were maintained. For the **hptp** compound, the coordinates of the atoms were obtained from the pdb file (code: 3zrm). Quantum chemistry calculation was carried out in order to generate the RESP charge of the ligand. The calculation was carried out at the level of HF/6–31G* using the Gaussian 03 program [69]. The results were input into the Amber package in order to derive the atomic charges of the ligands by following the Amber manual [68] with the antechamber module [70]. The partial charges of the atoms in the **hptp** compound are listed in Table S1 in the supporting information. Other force field parameters were obtained from the gaff force field and the parmchk module. The Amber ff03.r1 force field was used for the protein. The force field for the phosphorylated tyrosine was imported following the Amber manual [68]. Five Cl[–] ions were added to neutralize the net charge of the protein. A rectangular box of TIP3P water molecules was added such that the minimum distance of any solute atom to the walls of the box was 12 Å. In total, the complex state simulation involved 67,788 atoms. As for analog **1**, the atomic coordinates were obtained by substituting a phenyl group from the **hptp** compound with a –Br group using the DSviewer program. To generate the force-field parameters for analog **1**, a computational procedure similar to that of the **hptp** compound was conducted. Finally, the topology and coordinate files for the analog were prepared following the procedure in the Amber11 manual [68]. For the solution-state computations, we employed a procedure similar to what was used to generate the topology and coordinate files for the complex state. As for the investigations of the other analogs, their structures were generated using a procedure that was similar to the one used to generate analog **1**, and the resultant atomic coordinates were used to generate the force-field parameters and as the initial structure for the energy minimization and MD simulation. The other simulation procedures were similar to the ones used for analog **1**.

In computing ΔG , the mutation of **hptp** into its analog was divided into three steps, which followed the Amber11 manual [68]. First, we switched off the electrostatic interactions of the atoms of **hptp** that differ from those of its analog by switching the partial charges to zero. Second, the atoms of **hptp** differing from those of its analog were made to “disappear” and the atoms of its analog differing from those of **hptp** were made to “appear,” using the soft core potential scheme of van der Waals (vdw) interactions [68]. Third, we switched on the partial charges of the atoms of the analog that differed from those of **hptp** to complete the mutation.

With the topology and coordinate files in hand, we subjected the system to an energy minimization of 4000 steps with the steepest descent method and 1000 steps with the conjugate gradient method, followed by an NTV MD simulation for 10 ps with an initial temperature of 10 K and a target temperature of 300 K, using the Amber default random number seed for atom velocity assignment. We performed a subsequent NTP MD simulation for 250 ps

as an equilibration run. MD simulations for a further 600 ps were performed as production runs and used to calculate $\langle dV/d\lambda \rangle_\lambda$ and the resultant values of ΔG_{mut} . The $dV/d\lambda$ value was collected every 0.2 ps for each run, resulting in a total of 3000 data points for further analysis. For a number of cases, the simulation was extended to 1200 ps for a convergence check in the course of searching for better inhibitors or in the later stages of the project because of the availability of increased computer power. In the MD simulations, all bonds associated with hydrogen atoms were constrained at their equilibrium bond lengths with a time step of 2 fs. For the second mutational step, the noshakemask was turned on to mask those mutating atoms due to the use of the soft-core potential [68]. Similar to the results in our previous work [49], the second step of the vdw transformation in the complex state had a large fluctuation in the calculated ΔG . To obtain better convergence, 6 independent trajectories typically give reasonable converged values with an estimated error bar of 0.5 kcal/mol. We therefore carried out the same simulation except that the random number seeds for atomic velocity assignments were different for the remaining 5 trajectories. In the case of analog **5**, two more independent trajectories were added for better convergence. It was noted that a simulation length of longer than a nanosecond is ideal for obtaining better sampling. However, due to limited computer power, the present simulations were carried out only on a nanosecond scale. Previous studies have shown that, in computing relative and absolute binding free energy calculations for ligand–protein complexes, in general a simulation with a length on the order of 10 ns will give values for binding free energy with a higher precision and accuracy level (see articles [10,71] and references therein). MD simulation on the order of a nanosecond in length is expected to be too short to produce high precision and accuracy in many cases. However, this problem may be avoided in relative binding free energy calculation if the effect of conformational change in the binding free energy for the pair of ligands investigated is the same [10]. Our previous study showed that multiple short trajectories of 1.2 ns gave results comparable to those obtained from a single long trajectory of 9 ns, with only a small difference of 0.6 kcal/mol [49]. This indicated that multiple short trajectories gave results comparable to those obtained from

Table 1
Calculated free energy changes for analog **1** (kcal/mol).

Mutational step	Complex state	Solution state	$\Delta \Delta G$	Exp. ^a
1	18.2	18.4		
2	−21.8	−23.0		
3	−0.1	−0.1		
Total	−3.7	−4.7	1.0	−0.1

^a Converted from experimental values of pIC_{50} values which are 6.9 and 6.8, respectively [61].

the single long trajectory for the investigated ERK kinase-inhibitor complexes [49]. In addition, the use of multiple short trajectories is supported by previous studies of MD simulations (see, for example, the article [72]).

2.3. Hydrogen bond calculation

Because the λ points at 0.1, 0.2, ..., 0.9 were computed in MD simulations for the **hptp** compound, the hydrogen bonds between the ligand and the protein were computed using the trajectory of a production run at $\lambda = 0.1$ in the first mutational step of turning the charge off. This trajectory is the one closest to the **hptp** compound. In a similar manner, for the analogs, hydrogen bonds were obtained from the trajectory at $\lambda = 0.9$ in the third mutation step of turning the charge back on. The criterion for the hydrogen bond formation $X-H \cdots Y$, where X/Y is either an O or a N atom, must satisfy two conditions: (1) the distance between X and Y atoms must be $< 3.5 \text{ \AA}$; and, (2) the angle of $X-H-Y$ must be $> 120^\circ$. Snapshots of trajectories forming hydrogen bonds (h-bond) were calculated and are presented with the percentages of total snapshots.

3. Results and discussion

3.1. Calculated $\Delta \Delta G$ for the pair of available experimental data

The calculated ΔG for each step in the complex and the solution states for the **hptp** compound and analog **1** are listed in Table 1. It was noted that, of those 6 computed ΔG values (3 steps of

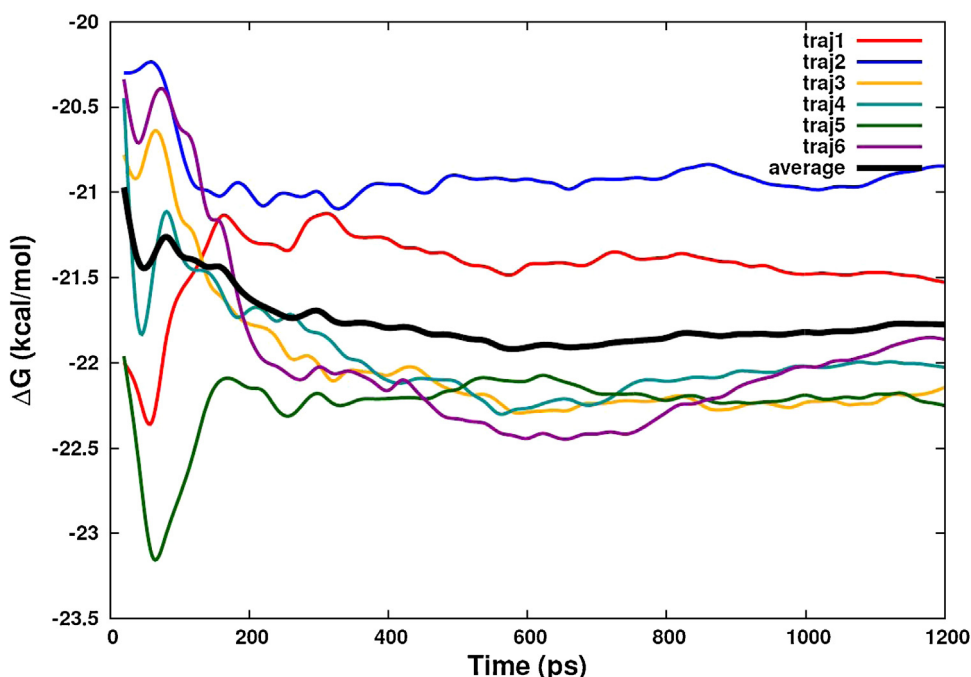


Fig. 3. Simulation length dependence of calculated ΔG of the second mutational step in the complex state for **hptp** and **1** compounds. traj1 denotes the 1st trajectory, etc. The black line is the average of those 6 trajectories.

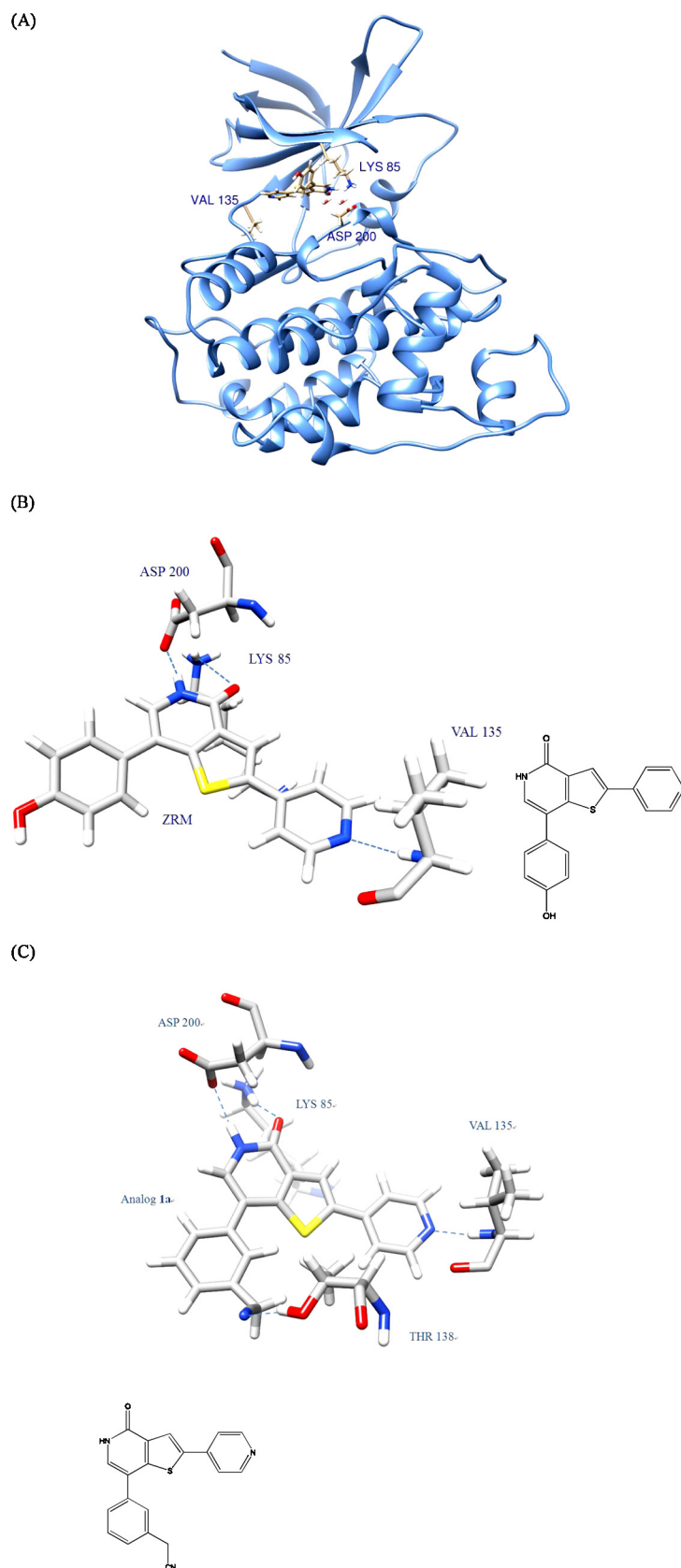
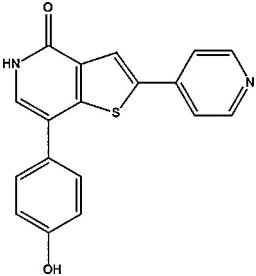
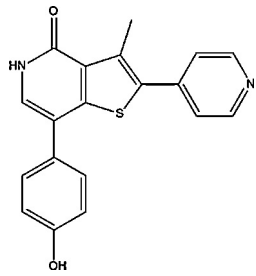
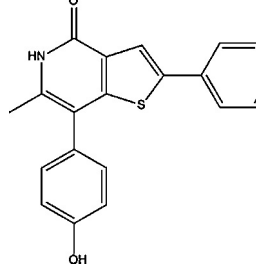
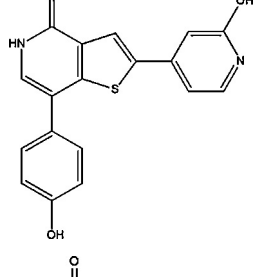
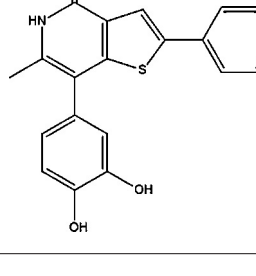


Fig. 4. (A) Binding of the **hptp** compound with GSK3 β kinase (see text for detailed description). (B) Hydrogen bonding of **hptp** compound with GSK3 β kinase at the binding site in simulation. Percentages of hydrogen bonds with Val135, Asp200, and water molecules inside the binding pocket present in the trajectory were 98, 97, and 99%, respectively. Hydrogen bonding with Lys85 with a minor strength of 35% present in the trajectory was observed. Hydrogen bonding in simulation were in agreement with the experimental results observed in a crystal structure [61]. (C) Hydrogen bonding of compound **1a** with GSK3 β kinase at the binding site in simulation. One additional h-bond with Thr138 was observed (see text for detailed description).

Table 2
Predicted values for $\Delta\Delta G$ (kcal/mol) for new analogous ligands, which uses the **hptp** compound as a reference. Values of calculated ΔG for each step in complex and solution states are listed in the supporting information. A negative $\Delta\Delta G$ value equates to a better binding affinity compared with the reference **hptp** compound.

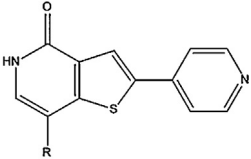
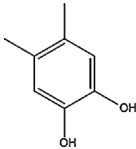
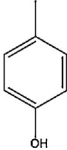
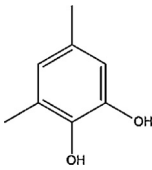
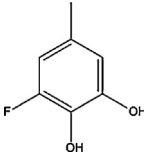
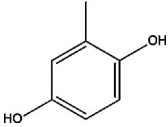
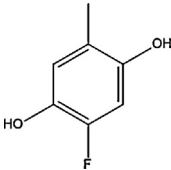
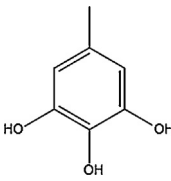
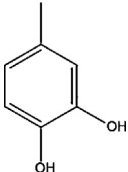
Ligand scaffold	Analog	Structure	$\Delta\Delta G$
			
hptp			
	2		0.4
	3		0.2
	4		2.2
	5		−0.5

complex state and 3 steps of solution state), the calculated ΔG s converged well in a single trajectory, with the exception of the second mutational step of vdw transformation in the complex state. The results where the ΔG s of those 5 well-converged computations obtained from the 250 ps equilibration runs and the 600 or 1200 ps production runs were essentially the same, and indicated a convergence in those computations. For the second mutational step in the complex state, the simulation time dependence of the calculated ΔG is shown in Fig. 3. The curve of the average went flat after ~600 ps indicating convergence. All these calculated ΔG 's resulted in a $\Delta\Delta G$ of 1.0 kcal/mol, which was in reasonably good agreement with the experimental value of −0.1 kcal/mol. The computed value differs from experimental value by +1.1 kcal/mol. The error bar was estimated at 0.5 kcal/mol based on the pattern of an average curve of 6 trajectories for the second mutational step in the complex state, which was similar to our previous study that also used confidence interval analysis [73] to assist in estimating the error bar and demonstrating how error bars decrease as simulation time increases [49]. The error bar of the experimental results is not

available. In addition to the calculated $\Delta\Delta G$, a computation of the h-bonds between the ligand and the protein environment showed that the **hptp** compound formed an h-bond with Val135 with a 99% presence of the h-bond in the trajectory. The binding of the **hptp** compound with GSK3 β kinase and the h-bonds between them in the MD simulation is shown in Fig. 4(A) and (B), respectively. A summary of the percentages of the h-bonds between the ligands and the protein in the trajectories is given in Table S2 of the supporting information. The h-bond with Val135 located in the hinge region of the kinase is the signature h-bond of kinase inhibitors binding with kinases. The oxygen atom of the fused ring also interacted with Lys85 with a lower percentage (38%) of h-bond formation. These h-bonds were also observed in the crystal structure [61]. Notably, in the simulation, a 97% presence of h-bonds with Asp200 was observed in the trajectory. However, this h-bond was not seen in the crystal structure due to the orientation of the side chain of Asp200 in the crystal structure, although Asp200 was in close proximity to the ligand [61]. The difference in the experimental structure might have been because the modeling was in a solution environment

Table 3

Predicted values for $\Delta\Delta G$ (kcal/mol) for new analogous ligands, which uses the **hptp** compound as a reference. Values of calculated ΔG for each step in complex and solution states are listed in the supporting information.

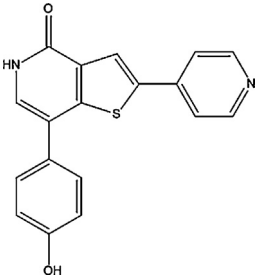
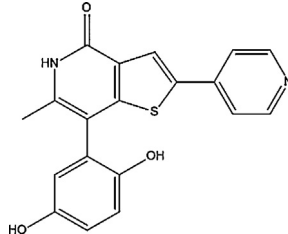
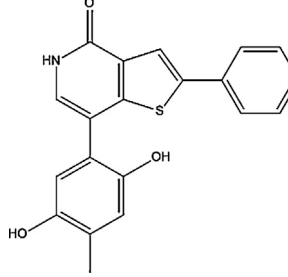
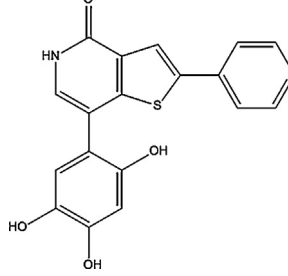
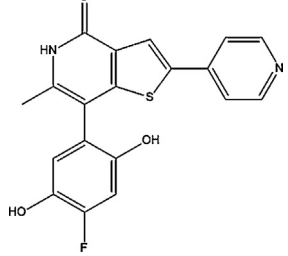
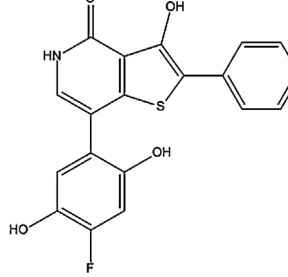
Ligand scaffold	Analog	R group	$\Delta\Delta G$
	6		1.0
	hptp		1.3
	7		0.6
	8		−0.6
	9		−0.8
	10		0.5
	11		0.5
	12		

rather than in a crystal environment, and/or to an inaccuracy in the force field. For analog **1**, the percentages of the above four h-bonds were 97, 90, 55, and 100%, respectively, showing similar hydrogen bonding patterns. Along with the examination of the h-bonds, the structure of the complex in the MD simulations remained close to the crystal structure with a root-mean-square deviation (RMSD) that ranged approximately from 1.0 to 1.5 Å.

In addition to analog **1**, we also computed another analog with affinity data available, named analog **1a**, which is shown in Fig. 4(C), with an experimental $\Delta\Delta G$ value of −1.5 kcal/mol [61]. The

computation gave a value of −1.1 kcal/mol, which agreed with the experimental result. Computed ΔG values for all steps and the figures for the simulation of the time dependence of ΔG for the second mutational step of the complex are shown in Table SA1a and in Fig. S1a in Supporting information, respectively. Hydrogen bond calculation showed that the percentages of the hydrogen bonds with Val135, Asp200, Lys85, Thr138, and water molecules inside the binding pocket present in the trajectory (only >50% are discussed here) as 100, 99, 56, 94, and 92%, respectively. The hydrogen-bonding pattern was similar to the **hptp** compound

Table 4
 Predicted values for $\Delta\Delta G$ (kcal/mol) for new analogous ligands, which uses the **hptp** compound as a reference. The values of the calculated ΔG for each step in the complex and solution states are listed in the supporting information, with the exception of analog **16**.

Ligand scaffold	Analog	Structure	$\Delta\Delta G$
			
hptp			
	13		−0.2
	14		−0.8
	15		−1.7
	16		−1.2
	17		−2.2

described above with the exception of the interaction of the long $-\text{CH}_2\text{CN}$ functional group at the meta position of the benzene ring with Thr138. This result suggests that introducing a polar group at the meta position adds additional hydrogen bonding interactions with GSK3 β kinase, as well as enhancing affinity. All these results indicated that the present computational protocol gave results that were in reasonable agreement with the experimental results.

We therefore employed the same computational protocol in order to predict the $\Delta\Delta G$ of other analogs using the **hptp** compound as a reference. We started with making small modifications in order to explore if the substitutions would enhance affinity during the course of our search for better inhibitors. We first explored the modifications with a substitution at various sites inside the binding pocket.

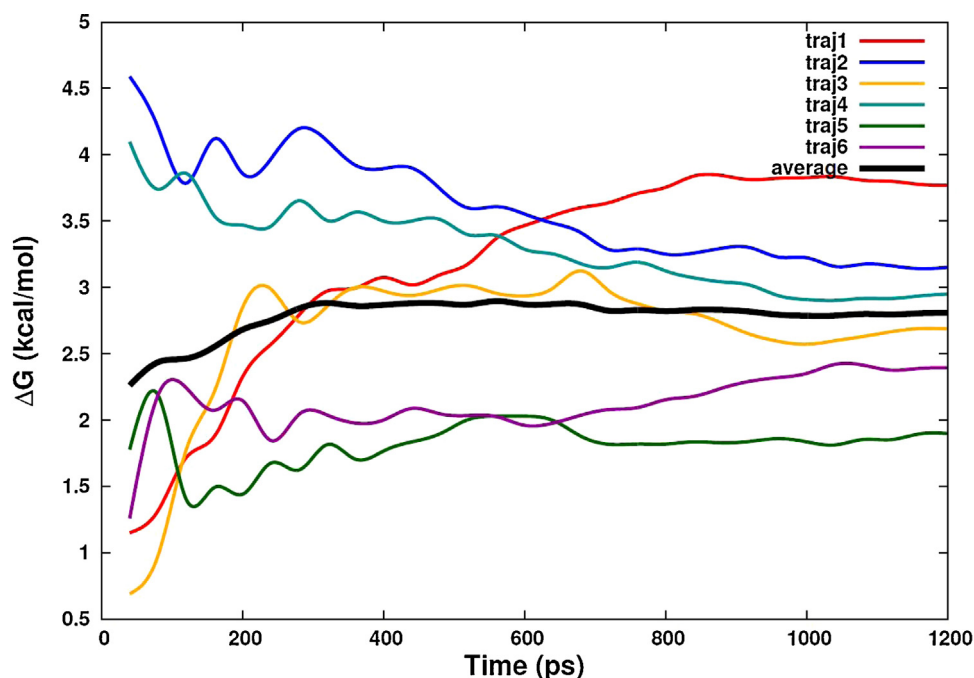


Fig. 5. Simulation length dependence of the calculated ΔG for the second mutational step in the complex state for **hptp** and analog **16** compounds. traj1 denotes the 1st trajectory, etc. The black line is the average of those 6 trajectories.

3.2. Substitutions at one selected site inside the binding pocket

The 4 investigated analogs are listed in Table 2 along with their $\Delta\Delta G$ values. The more negative the value, the stronger the affinity by comparison with the **hptp** reference compound. The 6 ΔG values of the 3 mutational steps in the complex and the solution states for each analog are listed in the tables in the supporting information along with the figures for the simulation of the time dependence of the ΔG values of the second mutational step in the complex state. These analogs were investigated because of the small spaces in the substitution sites in the binding pocket. The substitutions were thought to likely enhance affinity. However, the computations did not give the affinity for a significant enhancement. Although analog **5** had a $\Delta\Delta G$ value of -0.5 kcal/mol, it remained within the error bar of ~ 0.5 kcal/mol. As far as we could ascertain, data for the experimental binding affinity of the predicted ligands binding with GSK3 β kinase in the present study are not available. Calculations of the hydrogen bonds between the ligands and the protein environment showed that their hydrogen bonding patterns were similar to that of the **hptp** compound (see Table S2 in the supporting information). Computations for these investigated analogs did not enhance affinity compared with the **hptp** reference compound. We therefore shifted our attention to the phenyl ring that is located at the outer part of the binding pocket and points toward bulk water.

3.3. Substitutions at the phenyl ring

The computations for the $\Delta\Delta G$ of the 7 examined analogs are listed in Table 3. Among these analogs, with $\Delta\Delta G$ values of -0.6 and -0.8 kcal/mol, respectively, analogs **9** and **10** had better affinity than that of the **hptp** compound. Both had one additional $-OH$ group at the meta position on the left side of the benzene ring shown in the structures in the table combined with an additional $-OH$ group at the ortho position on the right side of the benzene ring. With respect to the hydrogen-bonding pattern, no obvious characteristic was observed. However, for 4 of the analogs (**6**, **8**, **9**, and **10**), simulations showed that adding $-OH$ groups on the

phenyl ring added h-bond(s) with Gln185 and/or Asn64. The other 3 analogs (**7**, **11**, and **12**) showed no additional hydrogen bond(s) either with Gln185 or Asn64. It was noted that these 3 analogs and analog **8** had no $-OH$ group at the ortho position and that the 3 substituted groups on the benzene ring were all located at the meta and para positions. This may be why these analogs had no h-bond(s) with either Gln185 and/or Asn64. Nevertheless, the main focus was to search for inhibitors that were better than the **hptp** compound. Therefore, analogs **9** and **10** were the main focus. The two computed $\Delta\Delta G$ values with better affinity suggested that the addition of two $-OH$ groups at the positions shown in analogs **9** and **10** significantly enhanced the affinity with GSK3 β kinase. We therefore carried out simulations for a few analogs with this characteristic.

3.4. Five more analogs with two $-OH$ groups in analogs **9** and **10**

The 5 investigated analogs and their $\Delta\Delta G$ values are listed in the Table 4. The first analog, analog **13**, had an additional methyl group on the inside of a binding pocket and did not significantly enhance affinity, which resulted in a lower affinity compared with analogs **9** and **10**, as described in the subsection 3.3. This showed that the addition of a methyl group at this position does not enhance affinity. It is noteworthy that with the presence of either a methyl, an OH, or an F group at the para position in the analogs **14**, **15**, **16**, and **17**, respectively, the computations gave $\Delta\Delta G$ values of -0.8 , -1.7 , -1.2 , and -2.2 kcal/mol, respectively. Fig. 5 shows the time dependence of the ΔG value of the second mutational step in the complex state for analog **16**, which was a well-converged

Table 5
Calculated free energy changes for analog **16** (kcal/mol).

Mutational step	Complex state	Solution state	$\Delta\Delta G$
1	11.9	11.8	
2	2.8	2.3	
3	-24.8	-23.0	
Total	-10.1	-8.9	-1.2

Table 6

Hydrogen bonding of ligands with Gln185 and Asn64 of GSK3 β kinase. The values under the residue names are the percentages of the hydrogen bonds between that residue and the ligands present in the production run trajectory (see text for detailed description).

Compound	Gln185	Asn64
hptp	0	1.75
1	0	0
2	0	0
3	0	0
4	0	0
5	97.83	0
6	88.33	0
7	0	0
8	0	44.49
9	24.25	46
10	63.83	0
11	0	0
12	0	0
13	82.25	44.75
14	97.83	74.67
15	1.92	81.67
16	97.58	82.83
17	86.17	0

result. The calculated ΔG values for all steps are listed in Table 5. In Table 6, the populations of h-bond formations with Gln185 and Asn64 for these 5 investigated analogs are listed and compared with those of other analogs. Examples of the h-bonding of analog **16** with GSK3 β kinase are representative of this characteristic, and are shown in Fig. 6. Table 6 shows that the investigated 5 analogs all had relatively high percentages of h-bond formations with Gln185 and/or Asn64 in the trajectories except analog **17** with Asn64, suggesting that the enhanced affinity could be attributed mainly to the formation of h-bond(s) with Gln185 and/or Asn64. Analog **13**, however, had a $\Delta \Delta G$ value of only -0.2 kcal/mol. It is noted here that, the percentages of h-bond populations do not correlate with binding affinity completely. Other interactions, for example, hydrophobic effect which is not straightforward to characterize quantitatively, may play some role in the computed affinity values. Another possible contributor may be the displacement of crystal water molecules around the phenol ring [74].

To investigate this issue, we first looked at whether the water molecules close to the phenol ring stayed close to the phenol ring in the 1200 ps production run of the reference compound-GSK3 β kinase complex. Because the simulation was in a solution state (instead of a crystal state in which crystal structure is), 9 water molecules were found around the phenol ring at the beginning of the production run. After 1200 ps, all of them were diffused into water, showing that all of them were not ordered water molecules. To further confirm these results, we carried out room mean square fluctuation (RMSF) calculation for all O atoms of all water molecules. The RMSF values of these 9 water molecules ranged from 10 to 20 Å, showing a large degree of movement, and the water molecules with the 15 lowest RMSF values were not located in the binding site except for the 2 buried in the deep pocket of the binding site shown in Fig. S18(a) of the supporting information. This further confirmed that the water molecules in the binding pocket close to the phenol ring were not ordered water molecules. To compare with compounds **15**, **16**, and **17** whose predicted binding free energy were enhanced significantly, the 20 lowest RMSF values of the water molecules are shown in Fig. S18(b) of the supporting information. As shown, the reference compound had the lower RMSF value compared with the other 3 compounds. Based on these curves, it seemed natural to consider that the water molecules with RMSF values <3.5 Å to be ordered water molecules. Based on this, the reference compound had more ordered water molecules (but note that they were all located at other parts of the protein, not the binding site, with the noted exception of the 2 buried in the deep pocket of the binding site as are most of the ordered water molecules for the other 3 compounds.) Therefore, it was not the displacement of ordered water molecules at the binding site that contributed to the enhanced binding free energy in the present cases. The above analysis suggests that protein reorganization energy, also mentioned in the last paragraph of the conclusion section in the paper [74], may play a role in the enhanced binding free energy. However, precise quantification requires accurate solvation theory/computation (including solvation treatment for those ordered water molecules) and computation for all the snapshots in the production runs, which should be the subject of future study. Overall, the present results merely suggest a qualitative correlation of h-bond population with the affinities. Nevertheless,

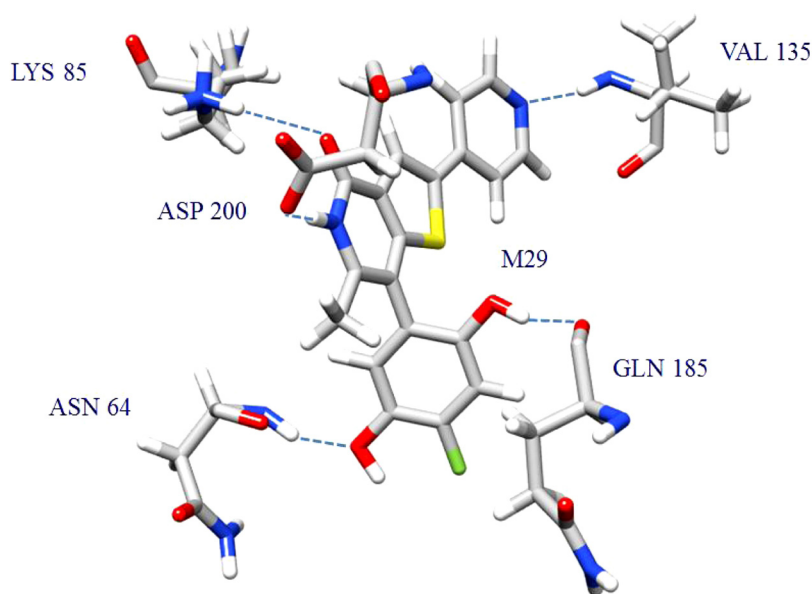


Fig. 6. Hydrogen bonding for analog **16** with GSK3 β kinase. The additional hydrogen bond(s) with Gln185 and/or Asn64 were characteristic interactions stabilizing the interactions between the analogs with an enhanced affinity for GSK3 β kinase. The examples of hydrogen bonding for analog **16** in this figure are representative of these analogs (see text for detailed description).

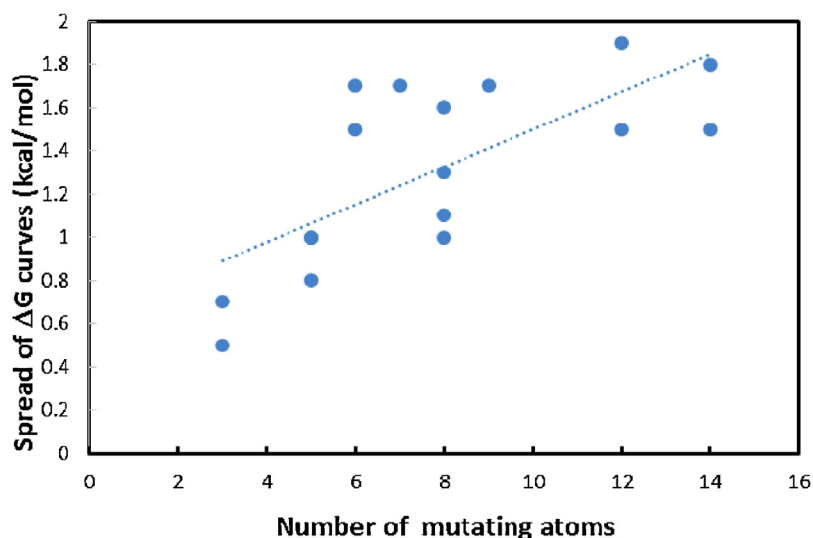


Fig. 7. Correlation of the number of mutating atoms with the spread of ΔG curves for the second mutational step of vdw transformation in the complex state. The number of mutating atoms refers to the sum of the number of atoms that 'disappeared' in the reference compound and the number of atoms that 'appeared' in the analogs.

these computed results were useful in rationalizing the interactions between the examined ligands and GSK3 β kinase that contributed to the enhanced affinity.

We noted here a technical point regarding how the number of mutating atoms relates to the spread of the curves for the computed ΔG obtained from the computed trajectories in the second mutational step of the complex state shown in Figs. 3 and 6 and in the figures in the supporting information. The extent of the spread of the independent trajectories in these figures was correlated with the magnitude of fluctuation in the calculated value. The spreads at the end of the production runs are listed in Table S3 in the supporting information along with the number of mutating atoms. These data are displayed in Fig. 7. The general trend shows how a greater number of mutating atoms equated to a larger spread. A quantitative, physical explanation, however, was not forthcoming. Nevertheless, these results showed how the curves of ΔG values might spread when a certain number of mutating atoms were chosen to mutate in TI-MD simulation using the present protocol. This analysis should be useful for MD simulation using an approach similar to the one presented in the present study. Regarding the experimental test for these predicted analogs, as this computational project went on during the research period, we found collaborative experimentalist in the later stage of the project. In addition, we also realized that these analogs are likely within claim of existing patent. We therefore shifted our focus on other new compounds of the same scaffold but are likely outside of patent claim for both computational and experimental works. These results will be reported in the future. Nevertheless, the computed results for binding affinity in the present study should be verified in future experiments. The predictions of analogs with better affinity should interest experimentalists working with enzyme and/or cell assays.

Finally, we noted one point for choosing the 3-step mutational protocol, used above, or the 1-step protocol in which electrostatic and vdw transformations were carried out separately or together, respectively, [68] taking analog **1** as an example. The 1-step computation gave a $\Delta\Delta G$ value of 1.0 kcal/mol, comparable with the value of 1.1 kcal/mol using the 3-step protocol. The computed ΔG values and convergence figure for complex computation are shown at the end of the supporting information. The present result supports usage of the 1-step computation. However, technically, the convergence of the 1-step protocol was slightly slower than that of the 3-step protocol in this case. In

addition, about twice the amount of CPU time is needed. This is because we experienced SHAKE (X-H bond constraints) failure when the 2 fs time step was used in all trajectories for all λ points when using the 1-step protocol, which required a 1 fs time step (this doubles CPU time) with the softcore potential turned on for vdw transformation. When the 3-step version was used, only about 30% of the trajectories had SHAKE failure. This information is useful in choosing between the 1-step and 3-step protocols.

4. Concluding remarks

TI MD simulation was utilized to find analogs of an existing reference inhibitor that would be better at binding with GSK3 β kinase. The first simulation for the pair with available experimental data gave a $\Delta\Delta G$ value of 1.0 kcal/mol, which was in reasonably good agreement with the experimental value of -0.1 kcal/mol. In the course of searching for substitutions that would create better inhibitors, the computations for another 16 analogs gave the three highest values of -2.2 , -1.7 , and -1.2 kcal/mol with another three values that ranged from -0.8 to -0.6 kcal/mol. Overall, the results showed that the addition of two $-OH$ groups on the benzene ring, one at the meta position and one at the ortho position, of analogs **14–17** shown in Table 4, significantly enhanced the binding affinity with GSK3 β kinase. Hydrogen bond analysis showed that these two additional $-OH$ groups each formed one additional h-bond(s) with Gln185 and/or Asn64, together or separately, compared with the reference **hptp** compound as well as with most other examined analogs of lower affinity. These results suggested that they were the main contributors to the enhanced affinity. Finally, the predicted affinity should be verified in future experiments, and the prediction of analogs with better affinity should interest experimentalists in future studies.

Acknowledgment

We thank the Ministry of Science and Technology of Taiwan for financial support. The authors also would like to acknowledge the National Center for High-performance Computing for providing huge computing resources to facilitate this research. Partial support from a NTNU new project grant is also acknowledged. Finally, we thank the NTNU English editing clinical service.

Appendix A. Supplementary data

Supplementary data associated with this article can be found, in the online version, at <http://dx.doi.org/10.1016/j.jmgm.2014.04.010>.

References

- [1] P. Cohen, Protein kinases – the major drug targets of the twenty-first century? *Nat. Rev. Drug Discov.* 1 (2002) 309–315.
- [2] D.L. Mobley, K.A. Dill, Binding of small-molecule ligands to proteins: what you see is not always what you get, *Structure* 17 (2009) 489–498.
- [3] Y.Q. Deng, B. Roux, Computations of standard binding free energies with molecular dynamics simulations, *J. Phys. Chem. B* 113 (2009) 2234–2246.
- [4] T. Steinbrecher, A. Labahn, Towards accurate free energy calculations in ligand protein-binding studies, *Curr. Med. Chem.* 17 (2010) 767–785.
- [5] W.L. Jorgensen, L.L. Thomas, Perspective on free-energy perturbation calculations for chemical equilibria, *J. Chem. Theory Comput.* 4 (2008) 869–876.
- [6] C.D. Christ, A.E. Mark, W.F. van Gunsteren, Feature article basic ingredients of free energy calculations: a review, *J. Comput. Chem.* 31 (2010) 1569–1582.
- [7] E. Gallicchio, R.M. Levy, in: C. Christov (Ed.), *Recent Theoretical and Computational Advances for Modeling Protein–Ligand Binding Affinities*, Elsevier Academic Press Inc., San Diego, USA, 2011.
- [8] A. de Ruiter, C. Oostenbrink, Free energy calculations of protein–ligand interactions, *Curr. Opin. Chem. Biol.* 15 (2011) 547–552.
- [9] M.R. Shirts, D.L. Mobley, J.D. Chodera, Alchemical free energy calculations: ready for prime time? *Ann. Rep. Comput. Chem.* 3 (2007) 41–59.
- [10] J.D. Chodera, D.L. Mobley, M.R. Shirts, R.W. Dixon, K. Branson, V.S. Pande, Alchemical free energy methods for drug discovery: progress and challenges, *Curr. Opin. Struct. Biol.* 21 (2011) 150–160.
- [11] D.A. Pearlman, P.S. Charifson, Are free energy calculations useful in practice? A comparison with rapid scoring functions for the P38 map kinase protein system, *J. Med. Chem.* 44 (2001) 3417–3423.
- [12] W.C. Yang, Y.M. Pan, L. Fang, D.Q. Gao, F. Zheng, C.G. Zhan, Free energy perturbation simulation on transition states and high-activity mutants of human butyrylcholinesterase for (–)-cocaine hydrolysis, *J. Phys. Chem. B* 114 (2010) 10889–10896.
- [13] P. Satpati, C. Clavaguera, G. Ohanessian, T. Simonson, Free energy simulations of a Gtpase: Gtp and Gdp binding to archaeal initiation factor 2, *J. Phys. Chem. B* 115 (2011) 6749–6763.
- [14] D.A. Pearlman, P.S. Charifson, Improved scoring of ligand–protein interactions using Owfeg free energy grids, *J. Med. Chem.* 44 (2001) 502–511.
- [15] F.R. Beierlein, G.G. Kneale, T. Clark, Predicting the effects of basepair mutations in DNA–protein complexes by thermodynamic integration, *Biophys. J.* 101 (2011) 1130–1138.
- [16] J. Fidelak, J. Juraszek, B. Branduardi, M. Bianciotto, F.L. Gervasio, Free-energy-based methods for binding profile determination in a congeneric series of Cdk2 inhibitors, *J. Phys. Chem. B* 114 (2010) 9516–9524.
- [17] Deng N.-j, P. Zhang, P. Cieplak, L. Lai, Elucidating the energetics of entropically driven protein–ligand association: calculations of absolute binding free energy and entropy, *J. Phys. Chem. B* 115 (2011) 11902–11910.
- [18] M. Kolár, P. Fanfrlík, J. Hobza, Ligand conformational and solvation/desolvation free energy in protein–ligand complex formation, *J. Phys. Chem. B* 115 (2011) 4718–4724.
- [19] I.J. General, R. Dragomirova, H. Meirovitch, New method for calculating the absolute free energy of binding: the effect of a mobile loop on the avidin/biotin complex, *J. Phys. Chem. B* 115 (2010) 168–175.
- [20] J.E. Elenewski, J.C. Hackett, Free energy landscape of the retinol/serum retinol binding protein complex: a biological host–guest system, *J. Phys. Chem. B* 114 (2010) 11315–11322.
- [21] A. Pohorille, C. Jarzynski, C. Chipot, Good practices in free-energy calculations, *J. Phys. Chem. B* 114 (2010) 10235–10253.
- [22] X.X. Ge, B. Roux, Absolute binding free energy calculations of sparsomycin analogs to the bacterial ribosome, *J. Phys. Chem. B* 114 (2010) 9525–9539.
- [23] D.L. Mobley, A.P. Graves, J.D. Chodera, A.C. Reynolds, B.K. Shoichet, K.A. Dill, Predicting absolute ligand binding free energies to a simple model site, *J. Mol. Biol.* 371 (2007) 1118–1134.
- [24] H. Fujitani, Y. Tanida, M. Ito, G. Jayachandran, C.D. Snow, M.R. Shirts, E.J. Sorin, V.S. Pande, Direct calculation of the binding free energies of Fkbp ligands, *J. Chem. Phys.* 123 (2005) 084108.
- [25] J.Y. Wang, Y.Q. Deng, B. Roux, Absolute binding free energy calculations using molecular dynamics simulations with restraining potentials, *Biophys. J.* 91 (2006) 2798–2814.
- [26] M.S. Lee, M.A. Olson, Calculation of absolute protein–ligand binding affinity using path and endpoint approaches, *Biophys. J.* 90 (2006) 864–877.
- [27] G. Jayachandran, M.R. Shirts, S. Park, V.S. Pande, Parallelized-over-parts computation of absolute binding free energy with docking and molecular dynamics, *J. Chem. Phys.* 125 (2006) 084901.
- [28] T. Steinbrecher, D.A. Case, A. Labahn, A multistep approach to structure-based drug design: studying ligand binding at the human neutrophil elastase, *J. Med. Chem.* 49 (2006) 1837–1844.
- [29] T. Steinbrecher, D.L. Mobley, D.A. Case, Nonlinear scaling schemes for Lennard–Jones interactions in free energy calculations, *J. Chem. Phys.* 127 (2007) 214108.
- [30] S. Krapp, T. Kosłowski, T. Steinbrecher, The thermodynamics of charge transfer in DNA photolyase: using thermodynamic integration calculations to analyse the kinetics of electron transfer reactions, *Phys. Chem. Chem. Phys.* 12 (2010) 9516–9525.
- [31] T. Steinbrecher, A. Hrenn, K.L. Dormann, I. Merfort, A. Labahn, Bornyl (3,4,5-trihydroxy)-cinnamate – an optimized human neutrophil elastase inhibitor designed by free energy calculations, *Bioorg. Med. Chem.* 16 (2008) 2385–2390.
- [32] J.W. Pitera, W.F. van Gunsteren, A comparison of non-bonded scaling approaches for free energy calculations, *Mol. Simul.* 28 (2002) 45–65.
- [33] M.R. Shirts, V.S. Pande, Solvation free energies of amino acid side chain analogs for common molecular mechanics water models, *J. Chem. Phys.* 122 (2005) 134508.
- [34] T.C. Beutler, A.E. Mark, R.C. Vanschaik, P.R. Gerber, W.F. van Gunsteren, Avoiding singularities and numerical instabilities in free-energy calculations based on molecular simulations, *Chem. Phys. Lett.* 222 (1994) 529–539.
- [35] M. Zacharias, T.P. Straatsma, J.A. McCammon, Separation-shifted scaling, a new scaling method for Lennard–Jones interactions in thermodynamic integration, *J. Chem. Phys.* 100 (1994) 9025–9031.
- [36] D. Jiao, P.A. Golubkov, T.A. Darden, P. Ren, Calculation of protein–ligand binding free energy by using a polarizable potential, *Proc. Natl. Acad. Sci. U.S.A.* 105 (2008) 6290–6295.
- [37] J. Michel, M.L. Verdon, J.W. Essex, Protein–ligand complexes: computation of the relative free energy of different scaffolds and binding modes, *J. Chem. Theory Comput.* 3 (2007) 1645–1655.
- [38] J. Michel, J.W. Essex, Prediction of protein–ligand binding affinity by free energy simulations: assumptions, pitfalls and expectations, *J. Comput. Aided Mol. Des.* 24 (2010) 639–658.
- [39] J. Michel, N. Foloppe, J.W. Essex, Rigorous free energy calculations in structure-based drug design, *Mol. Inf.* 29 (2010) 570–578.
- [40] S. Genheden, I. Nilsson, U. Ryde, Binding affinities of factor Xa inhibitors estimated by thermodynamic integration and Mm/Gbsa, *J. Chem. Inf. Model.* 51 (2011) 947–958.
- [41] A. de Ruiter, C. Oostenbrink, Efficient and accurate free energy calculations on trypsin inhibitors, *J. Chem. Theory Comput.* 8 (2012) 3686–3695.
- [42] J.C. Gumbart, B. Roux, C. Chipot, Standard binding free energies from computer simulations: what is the best strategy? *J. Chem. Theory Comput.* 9 (2013) 794–802.
- [43] E. Gallicchio, R.M. Levy, Advances in all atom sampling methods for modeling protein–ligand binding affinities, *Curr. Opin. Struct. Biol.* 21 (2011) 161–166.
- [44] L. Wang, B.J. Berne, R.A. Friesner, On achieving high accuracy and reliability in the calculation of relative protein–ligand binding affinities, *Proc. Natl. Acad. Sci. U.S.A.* 109 (2012) 1937–1942.
- [45] D.L. Mobley, Let's get honest about sampling, *J. Comput. Aided Mol. Des.* 26 (2012) 93–95.
- [46] R.H. Zhou, P. Das, A.K. Royyuru, Single mutation induced H3n2 hemagglutinin antibody neutralization: a free energy perturbation study, *J. Phys. Chem. B* 112 (2008) 15813–15820.
- [47] G.J. Rocklin, D.L. Mobley, K.A. Dill, Separated topologies – a method for relative binding free energy calculations using orientational restraints, *J. Chem. Phys.* 138 (2013), Article no. 085104.
- [48] T. Steinbrecher, D.A. Case, A. Labahn, Free energy calculations on the binding of novel thiolactomycin derivatives to *E. coli* fatty acid synthase I, *Bioorg. Med. Chem.* 20 (2012) 3446–3453.
- [49] K.W. Wu, P.C. Chen, J. Wang, Y.C. Sun, Computation of relative binding free energy for an inhibitor and its analogs binding with ERK kinase using thermodynamic integration MD simulation, *J. Comput. Aided Mol. Des.* 26 (2012) 1159–1169.
- [50] S. Zhu, S.M. Travis, A.H. Elcock, Accurate calculation of mutational effects on the thermodynamics of inhibitor binding to P38 alpha map kinase: a combined computational and experimental study, *J. Chem. Theory Comput.* 9 (2013) 3151–3164.
- [51] I.J. General, H. Meirovitch, Absolute free energy of binding and entropy of the Fkbp12-Fk506 complex: effects of the force field, *J. Chem. Theory Comput.* 9 (2013) 4609–4619.
- [52] Z. Muhammed, S. Arai, S. Saijo, I. Yamato, T. Murata, A. Suenaga, Calculating the Na⁺ translocating V-ATPase catalytic site affinity for substrate binding by homology modeled Ntpa monomer using molecular dynamics/free energy calculation, *J. Mol. Graph. Model.* 37 (2012) 59–66.
- [53] B.L. Oliveira, I.S. Moreira, P.A. Fernandes, M.J. Ramos, I. Santos, J.D.G. Correia, Theoretical studies on the binding of rhenium(I) complexes to inducible nitric oxide synthase, *J. Mol. Graph. Model.* 45 (2013) 13–25.
- [54] H. Park, Y.H. Jeon, Free energy perturbation approach for the rational engineering of the antibody for human hepatitis B virus, *J. Mol. Graph. Model.* 29 (2011) 643–649.
- [55] J.W. Kaus, L.T. Pierce, R.C. Walker, J.A. McCammon, Improving the efficiency of free energy calculations in the AMBER molecular dynamics package, *J. Chem. Theory Comput.* 9 (2013) 4131–4139.
- [56] D.L. Mobley, P.V. Klimovich, Perspective: alchemical free energy calculations for drug discovery, *J. Chem. Phys.* 137 (2012), Article no. 230901.
- [57] G.J. Rocklin, D.L. Mobley, K.A. Dill, Calculating the sensitivity and robustness of binding free energy calculations to force field parameters, *J. Chem. Theory Comput.* 9 (2013) 3072–3083.

- [58] P.V. Klimovich, D.L. Mobley, Predicting hydration free energies using all-atom molecular dynamics simulations and multiple starting conformations, *J. Comput. Aided Mol. Des.* 24 (2010) 307–316.
- [59] M.T. Geballe, A.G. Skillman, A. Nicholls, J.P. Guthrie, P.J. Taylor, The Sampl2 blind prediction challenge: introduction and overview, *J. Comput. Aided Mol. Des.* 24 (2010) 259–279.
- [60] S. Liu, Y.J. Wu, T. Lin, R. Abel, J.P. Redmann, C.M. Summa, V.R. Jaber, N.M. Lim, D.L. Mobley, Lead optimization mapper: automating free energy calculations for lead optimization, *J. Comput. Aided Mol. Des.* 27 (2013) 755–770.
- [61] G. Gentile, G. Bernasconi, A. Pozzan, G. Merlo, P. Marzorati, P. Bamborough, B. Bax, A. Bridges, C. Brough, P. Carter, G. Cutler, M. Neu, M. Takada, Identification of 2-(4-pyridyl)thienopyridinones as Gsk-3 beta inhibitors, *Bioorg. Med. Chem. Lett.* 21 (2011) 4823–4827.
- [62] S. Amar, R.H. Belmaker, G. Agam, The possible involvement of glycogen synthase kinase-3 (Gsk-3) in diabetes, cancer and central nervous system diseases, *Curr. Pharm. Des.* 17 (2011) 2264–2277.
- [63] S.Y. Lu, Z.M. Huang, W.K. Huang, X.Y. Liu, Y.Y. Chen, T. Shi, J. Zhang, How calcium inhibits the magnesium-dependent kinase Gsk3 beta: a molecular simulation study, *Proteins* 81 (2013) 740–753.
- [64] S.Y. Lu, Y.J. Jiang, J. Lv, J.W. Zou, T.X. Wu, Mechanism of kinase inactivation and nonbinding of fratide to Gsk3 beta due to K85m mutation: molecular dynamics simulation and normal mode analysis, *Biopolymers* 95 (2011) 669–681.
- [65] S.Y. Lu, Y.J. Jiang, J.W. Zou, T.X. Wu, Molecular modeling and molecular dynamics simulation studies of the Gsk3 Beta/Atp/substrate complex: understanding the unique P + 4 primed phosphorylation specificity for Gsk3 beta substrates, *J. Chem. Inf. Model.* 51 (2011) 1025–1036.
- [66] X.N. Tang, C.W. Lo, Y.C. Chuang, C.T. Chen, Y.C. Sun, Y.R. Hong, C.N. Yang, Prediction of the binding mode between Gsk3 beta and a peptide derived from Gskip using molecular dynamics simulation, *Biopolymers* 95 (2011) 461–471.
- [67] P. Kollman, Free-energy calculations – applications to chemical and biochemical phenomena, *Chem. Rev.* 93 (1993) 2395–2417.
- [68] D.A. Case, T. Darden, T.E. Cheatham, C. Simmerling, J. Wang, R.E. Duke, R. Luo, R.C. Walker, W. Zhang, K.M. Merz, B. Roberts, B. Wang, S. Hayik, A. Roitberg, G. Seabra, I. Kolossvary, K.F. Wong, F. Paesani, J. Vanicek, X. Wu, S.R. Brozell, T. Steinbrecher, H. Gohlke, Q. Cai, X. Ye, J. Wang, M.-J. Hsieh, G. Cui, D.R. Roe, D.H. Mathews, M.G. Seetin, C. Sagui, V. Babin, T. Luchko, S. Vusarov, A. Kovalenko, P.A. Kollman, Amber 11, University of California, San Francisco, 2010.
- [69] M.J. Frisch, G.W. Trucks, H.B. Schlegel, G.E. Scuseria, M.A. Robb, J.R. Cheeseman, J.A. Montgomery Jr., T. Vreven, K.N. Kudin, J.C. Burant, J.M. Millam, S.S. Iyengar, J. Tomasi, V. Barone, B. Mennucci, M. Cossi, G. Scalmani, N. Rega, G.A. Petersson, H. Nakatsuji, M. Hada, M. Ehara, K. Toyota, R. Fukuda, J. Hasegawa, M. Ishida, T. Nakajima, Y. Honda, O. Kitao, H. Nakai, M. Klene, X. Li, J.E. Knox, H.P. Hratchian, J.B. Cross, V. Bakken, C. Adamo, J. Jaramillo, R. Gomperts, R.E. Stratmann, O. Yazyev, A.J. Austin, R. Cammi, C. Pomelli, J.W. Ochterski, P.Y. Ayala, K. Morokuma, G.A. Voth, P. Salvador, J.J. Dannenberg, V.G. Zakrzewski, S. Dapprich, A.D. Daniels, M.C. Strain, O. Farkas, D.K. Malick, A.D. Rabuck, K. Raghavachari, J.B. Foresman, J.V. Ortiz, Q. Cui, A.G. Baboul, S. Clifford, J. Cioslowski, B.B. Stefanov, G. Liu, A. Liashenko, P. Piskorz, I. Komaromi, R.L. Martin, D.J. Fox, T. Keith, M.A. Al-Laham, C.Y. Peng, A. Nanayakkara, M. Challacombe, P.M.W. Gill, B. Johnson, W. Chen, M.W. Wong, C. Gonzalez, J.A. Pople, Gaussian 03, Gaussian Inc., Wallingford, CT, 2004.
- [70] J.M. Wang, W. Wang, P.A. Kollman, D.A. Case, Automatic atom type and bond type perception in molecular mechanical calculations, *J. Mol. Graphics Model.* 25 (2006) 247–260.
- [71] D.L. Mobley, J.D. Chodera, K.A. Dill, Confine-and-release method: obtaining correct binding free energies in the presence of protein conformational change, *J. Chem. Theory Comput.* 3 (2007) 1231–1235.
- [72] S.K. Sadiq, D.W. Wright, O.A. Kenway, P.V. Coveney, Accurate ensemble molecular dynamics binding free energy ranking of multidrug-resistant Hiv-1 proteases, *J. Chem. Inf. Model.* 50 (2010) 890–905.
- [73] E. Kreyszig, *Advanced Engineering Mathematics*, Wiley, Hoboken, USA, 2005.
- [74] R. Abel, T. Young, R. Farid, B.J. Berne, R.A. Friesner, Role of the active-site solvent in the thermodynamics of factor Xa ligand binding, *J. Am. Chem. Soc.* 130 (2008) 2817–2831.
- [75] E.F. Pettersen, T.D. Goddard, C.C. Huang, G.S. Couch, D.M. Greenblatt, E.C. Meng, T.E. Ferrin, Ucsf Chimera – a visualization system for exploratory research and analysis, *J. Comput. Chem.* 25 (2004) 1605–1612.